Accepted Manuscript

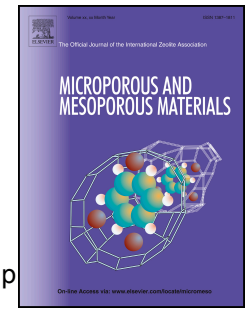

Visible light absorption of surface-modified Al_2O_3 powders: A comparative DFT and experimental study

Vesna Đorđević, Dušan N. Sredojević, Jasmina Dostanić, Davor Lončarević, S. Phillip Ahrenkiel, Nenad Švrakić, Edward Brothers, Milivoj Belić, Jovan M. Nedeljković

PII: S1387-1811(18)30363-9

DOI: 10.1016/j.micromeso.2018.06.053

Reference: MICMAT 9006

To appear in: *Microporous and Mesoporous Materials*

Received Date: 7 May 2018

Revised Date: 25 June 2018

Accepted Date: 28 June 2018

Please cite this article as: V. Đorđević, Duš.N. Sredojević, J. Dostanić, D. Lončarević, S.P. Ahrenkiel, N. Švrakić, E. Brothers, M. Belić, J.M. Nedeljković, Visible light absorption of surface-modified Al_2O_3 powders: A comparative DFT and experimental study, *Microporous and Mesoporous Materials* (2018), doi: 10.1016/j.micromeso.2018.06.053.

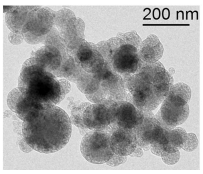

CAT/Al_2O_3

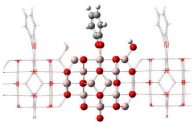

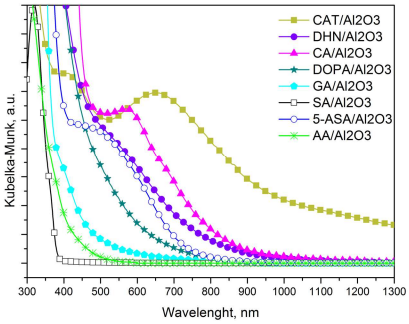

Visible Light Absorption of Surface-Modified Al_2O_3 Powders: A Comparative DFT and Experimental Study

Vesna Đorđević[a], Dušan N. Sredojević[a], Jasmina Dostanić[b], Davor Lončarević[b], S. Phillip Ahrenkiel[c], Nenad Švrakić[d], Edward Brothers[d], Milivoj Belić[d], Jovan M. Nedeljković[a,*]

[a] Institute of Nuclear Sciences Vinča, University of Belgrade, P.O. Box 522, 11001 Belgrade, Serbia

[b] Institute of Chemistry, Technology and Metallurgy, University of Belgrade, Studentski trg 12-16, 11000 Belgrade, Serbia

[c] South Dakota School of Mines and Technology, 501 E. Saint Joseph Street, Rapid City, SD 57701, USA

[d] Texas A&M University at Qatar, P.O. Box 23874, Doha, Qatar

*Corresponding author email: jovned@vinca.rs

Abstract

Surface modification of Al_2O_3 powders, prepared using reproducible sol-gel synthetic route with small colorless organic molecules, induces charge transfer complex formation and the appearance of absorption in the visible spectral region. Comprehensive microstructural characterization involving transmission electron microscopy, X-ray diffraction analysis, and nitrogen adsorption–desorption isotherms, revealed that γ-crystalline alumina powders consist of mesoporous particles

in the size range from 0.1 to 0.3 μm, with specific surface area of 54.8 m^2/g, and pore radius between 3 and 4 nm. The attachment of catecholate-type of ligands (catechol, caffeic acid, gallic acid, dopamine and 2,3-dihydroxy naphthalene), salicylate-type of ligands (salicylic acid and 5-amino salicylic acid), and ascorbic acid, to the surface such γ-Al_2O_3 particles leads to the formation of colored powders and activates their absorption in visible-light spectral region. To the best of our knowledge, similar transformation of an insulator (Al_2O_3), with the band gap energy of 8.7 eV, into a semiconductor-like hybrid material with tunable optical properties has not been reported in the literature before. The density functional theory (DFT) calculations with periodic boundary conditions were performed in order to estimate the energy gaps of various inorganic/organic hybrids. The calculated values compare well with the experimental data. The good agreement between the calculated and experimentally determined band gaps was found, thus demonstrating predictive ability of the theory when proper model is used.

Keywords: Charge transfer complex, Al_2O_3, Bidentate Benzene Derivatives, Visible light responsive material, Density functional theory.

1 Introduction

Wide band gap metal-oxides (TiO_2, ZnO_2, CeO_2 and SnO_2) have been extensively studied for the range of diverse applications because they are abundant, chemically stable, biocompatible, and readily affordable. In particular, numerous photo-driven processes – heterogeneous photocatalysis for removal of inorganic and organic pollutants, water splitting reaction, solar cells, etc. – using metal oxides have been extensively investigated in order to achieve desired level of practical efficiency [1–7]. However, the main disincentive for the use of oxide materials

in such applications is their large band gap. For example, the most studied metal-oxide photocatalyst, TiO_2, with the band gap of E_g=3.2 eV, absorbs less than 5% of the available solar photons, since only high-energy UV photons (λ<380 nm) are capable of generating electron-hole pairs that stimulate redox processes on the catalyst surface. Recently, considerable effort has been made to develop the visible-light responsive TiO_2 based materials. Basically, three different methods to extend absorption of TiO_2 into visible spectral region can be distinguished: dye sensitization [8, 9], doping with light and heavy elements [10, 11], and the use of plasmonic noble metal nanoparticles [12, 13].

More recently, a new method of tailoring optical properties of TiO_2, based on surface modification of this metal-oxide with small colorless organic molecules, has been developed. The use of ligand molecules, mainly benzene derivatives, leads to the formation of charge transfer complex (CTC) followed with the red-shift of absorption onset. It should be emphasized that there is a fundamental difference in photo-generation of charge carriers between the surface modification approach and sensitization with dye molecules. In the former case, electrons are in a single step directly injected from the ground state of the CTC, located in the semiconductor band gap, into the semiconductor conduction band, while the latter case involves two steps: first, the excitation of the dye molecules, and subsequent electron transfer from the excited state into the semiconductor conduction band. Until now, the CTC formation has been primarily studied using colloidal TiO_2 nanoparticles surface-modified with either catecholate- or salicylate-type of ligands [14–25]. Recently, the CTC formation between surface Ti atoms and organic mono-hydroxy compounds was reported [26, 27].

For many applications it is more convenient to use solid materials rather than colloidal solutions. To this end, spherical TiO_2 powder particles, prepared by using ultrasonic spray pyrolysis [28,

29], TiO_2 nano-powders prepared using sol-gel synthetic route, as well as commercial Degussa P25 powders [30], and polymer-supported TiO_2 nanoparticles [31], were successfully surface modified with catecholate- and salicylate-type of ligands. However, only a small number of studies regarding photocatalytic performance of surface-modified TiO_2 particles with extended absorption in visible spectral range were initiated. Thus far, hydrogen evolution over free-standing and polymer supported surface-modified TiO_2 particles has been reported [21, 31], as well as degradation of organic dyes using surface-modified TiO_2 with ascorbic acid [24] and catecholate-type of ligands [30–32]. Additionally, the photovoltaic performance of hybrid solar cell fabricated using surface-modified TiO_2 nanoparticles with 6-palmitate ascorbic acid as an electron acceptor embedded into the donor poly(3-hexyl)thiophene matrix was investigated [33]. Theoretical approaches via quantum chemical calculations based on density functional theory (DFT) have been used for determination of HOMO/LUMO gap values and infrared spectra of coordinated ligand molecules to metal-oxide surfaces [17–22, 25-27, 34–36]. Although the significant difference between theoretical and experimental values could frequently be observed, the calculated values followed the same general trend as experimental data.

Up until now, almost all investigations concerning tunable optical properties as a consequence of CTC formation have been performed using either colloidal TiO_2 nanoparticles or TiO_2 nano-powders. Very recent studies have shown that CTC formation is not exclusive of TiO_2, and that the CTC formation, followed with the red-shift of optical absorption, can be achieved using commercial $Na_2Ti_3O_7$ nanotubes [37], ZnO nanoparticles [22], Mg_2TiO_4 nano-powders [38], and $BaTiO_3$ nanoparticles [39]. However, the possibility to bring optical absorption in visible spectral range of inorganic/organic hybrids, consisting of solar light non-absorbing materials, i.e., insulators, and small colorless organic molecules, has never been tested. Our preliminary results

demonstrate that CTC formation takes place between surface of alumina powders and model ligand molecules (catechol and 5-amino salicylic acid), and that the resulting composites can perform photocatalytically [40]. Motivated by the fact that mesoporous Al_2O_3 materials have already attracted great deal of interest from industry and academia due to wide range of their applications, including catalysis, sensing, adsorption and separation [41, 42], in this work we present comprehensive experimental and theoretical study that provides basic understanding of transformation of an insulator with band gap energy of 8.7 eV [43] into a semiconductor-like hybrid with new potential functionality.

On the experimental side, thorough microstructural characterization of synthesized Al_2O_3 particles, including transmission electron microscopy (TEM), X-ray diffraction (XRD) analysis, and nitrogen adsorption–desorption isotherms was performed. Also, optical properties of hybrids obtained by modifying Al_2O_3 particles with catecholate-type of ligands (catechol, caffeic acid, gallic acid, dopamine and 2,3-dihydroxy naphthalene), salycilate-type of ligands (salicylic acid and 5-amino salicylic acid) and ascorbic acid were studied using reflection spectroscopy, while mode of coordination of ligand molecules to the surface of Al_2O_3 was examined using FTIR. On theoretical side, the DFT calculations with periodic boundary conditions were performed using bridging mode of binding of ligands to the surface Al atoms. The description of the procedures used and the summary of our main results are given in the sections that follow.

2 Experimental Procedures

2.1 Synthesis of surface-modified Al_2O_3 powders

All chemicals used in our experiments were of the highest purity available and were utilized without further purification (Alfa Aesar, J.T. Baker). Milli-Q deionized water was used as a solvent (resistivity 18.2 MΩ cm^{-1}).

The Al_2O_3 powders were prepared in a manner similar to the method described elsewhere [44]. Briefly, the round bottom flask with 20 mol of distilled water was heated in oil bath up to 85 °C, and 0.20 mol of aluminium isopropoxide ($Al[OCH(CH_3)_2]_3$) was added under vigorous stirring. After 15 minutes, 4.85 ml of nitric acid (HNO_3, 69-70%) was added and the solution was stirred and kept uncovered for 2 hours at 85 °C, giving the adequate time for isopropanol, formed during the hydrolysis, to evaporate. The covered flask was heated and stirred continuously for additional 4 hours. Then, 12.0 g of water soluble polymer Polyethylene glycol 12000 ($H(OCH_2CH_2)_nOH$, M.W. range 11,000 - 13,000) was added into the cooled solution and gentle stirring was maintained overnight. The obtained sol was dried in air in open beaker, heated to 70 °C, until viscous white gel was formed. The gel was then transferred into porcelain crucible and finally calcinated either at 700 or 1100 °C for 24 hours in open-air furnace.

Surface modification of Al_2O_3 powders was achieved by dispersing 0.1 g of powder in 10 ml of water containing adequate amount (1.53×10^{-5} mol) of dissolved ligands (L). It should be mentioned that the molar ratio between inorganic and organic components was the same for all prepared hybrids. For surface modification of γ-Al_2O_3 powders, catecholate-type of ligands (catechol (CAT), 2,3-dihydroxy naphthalene (DHN), caffeic acid (CA), dopamine (DOPA), gallic acid (GA)) and salicylate-type of ligands (salicylic acid (SA), 5-amino salicylic acid (5-ASA)) were used, as well as ascorbic acid (AA). After 2 days, the powders were separated by centrifugation, thoroughly washed three times with distilled water, and finally dried in the vacuum oven at 40 °C.

2.2 Structural characterization of surface-modified γ-Al_2O_3 powders

The X-ray diffraction (XRD) powder patterns were recorded using Rigaku SmartLab instrument under the Cu $K\alpha_{1,2}$ radiation. The intensity of diffraction was measured with continuous angular scanning at 2 °/min. The data were collected at 0.02° intervals. Transmission electron microscopy (TEM) imaging was performed using a JEOL JEM-2100 LaB_6 instrument operated at 200 kV. TEM images were acquired with a Gatan Orius CCD camera at 2× binning. Nitrogen adsorption-desorption isotherms were determined on Sorptomatic 1990 Thermo Finnigan automatic system using nitrogen physisorption at -196 °C. Before taking measurements, the samples were outgassed at 130 °C for 3 hours. Specific surface area of the samples was calculated from the nitrogen adsorption-desorption isotherms according to the BET method [45]. Pore size, pore volume distribution, and porosity were determined by mercury intrusion porosimetry on Pascal 140/440, Thermo Scientific. The content of organic phase in hybrid samples was determined by TGA using a Setaram Setsys Evolution-1750 instrument. The measurements were performed in temperature range 25–900 °C at a heating rate of 10 °C min^{-1}, in dynamic air atmosphere (flow rate 20 cm^3 min^{-1}).

Optical properties of surface-modified Al_2O_3 particles were studied in the wavelength range from 300 nm to 1.3 μm by diffuse reflectance measurements (Shimadzu UV-Visible UV-2600 spectrophotometer equipped with an integrated sphere ISR-2600 Plus). Infrared spectroscopy measurements were carried out using a Thermo Nicolet 6700 FTIR spectrometer at spectral resolution of 8 cm^{-1} in the region of 4000–400 cm^{-1}.

2.3 Computational details

The DFT calculations with periodic boundary conditions (PBC) were performed with the Gaussian 09 suite of programs [46]. The electronic exchange and correlation effects were included by means of the Heyd-Scuseria-Ernzerhof screened hybrid functional (HSE06) [47, 48]. We used the Pople 6-31G(d,p) valence double-zeta polarized basis set [49, 50], and the ultrafine integration grid was specified for all calculations. The unit cell, used for the periodic calculations, was constructed based on the defect-free crystal structure of γ-Al_2O_3 (7.887×7.887×7.887 Å). To model (1 0 1) Al_2O_3 surface, the appropriate slab model was employed that is partially hydroxylated, and includes capped oxygen atom on the bottom, in order to keep the Al_2O_3 stoichiometry and charge neutrality of the unit cells. The rectangular five-layered unit cell consisting of 14 aluminums and 21 oxygen atoms was periodically repeated along the two orthogonal directions defined by translation vectors of 7.887 and 5.649 Å. To mimic the electronic structures of various interfacial L/Al_2O_3 complexes, the ligand molecules were anchored on the top side of unit cells that represent the (1 0 1) surface of γ-Al_2O_3. This model assumes infinite vacuum space along the directions that is orthogonal to the translation vectors. The surface Brillouin zone was sampled by 98 Monkhorst-Pack k-points [51]. The optimization of the atomic coordinates was carried out within the unit cell by using Berny's algorithm, whereas the lattice parameters were fixed in all cases.

3 Results and Discussion

3.1 Microstructural and optical properties of surface-modified Al_2O_3 powders

The wide-angle XRD patterns of Al_2O_3 particles, prepared by a sol-gel process via hydrolysis of aluminum isopropoxide, followed with calcination are shown in Figure 1. The diffractogram of samples calcinated at 700 ^{0}C (Figure 1A) displayed the presence of three distinct broad peaks at

37.5, 45.9, and 67.1° that belong to (311), (400), and (440) planes of the crystalline γ-Al_2O_3, respectively (JCPDS Card No. 00-010-0425). The crystallite size, calculated from the widths of the XRD peaks by using the Debye-Scherrer equation, was found to be 32 Å. It should be noted that the presence of other coexisting alumina phases or impurities was not detected. On the other hand, calcinations at 1100 °C induced the appearance of sharp diffraction peaks (see Figure 1B) that belong to the corundum crystal structure (JCPDS Card No. 00-056-0457). This result is consistent with literature data indicating that above 1050 °C the γ-Al_2O_3 is being completely converted into α-Al_2O_3 [52].

The TEM characterization of γ-Al_2O_3 powders indicated the presence of fairly uniform spherically shaped particles in the size range from 0.1 to 0.3 μm. Dark-field TEM imaging, as well as closer inspection at higher magnifications, indicated that submicron-sized γ-Al_2O_3 spheres resemble a “dandelion” shape (see Figure 2) due to the presence of many nano-crystallites. Thus, there is a good agreement between the crystallite size obtained by the XRD measurements and by the TEM analysis of the γ-Al_2O_3 powders. Analysis of the selected area electron diffraction (SAED) pattern revealed the presence of the diffraction rings consistent with the crystalline γ-Al_2O_3 structure, including the (311), (400), and (440) planes.

Nitrogen adsorption-desorption isotherm of synthesized γ-Al_2O_3 samples and pore size distribution are shown in Figure 3 (curves a and b, respectively). The specific surface area was calculated using BET method [45], and was found to be 54.8 m^2/g. The pore radius was estimated using BJH method [53]. The determined pore radius in the size range from 3 to 4 nm clearly indicates that γ-Al_2O_3 samples are mesoporous.

The surface-modification of Al_2O_3 samples calcinated at 700 °C (γ-phase) with catecholate- and salicylate-type of ligands, as well as with AA induce coloration of powders due to CTC

formation. Note that, under identical experimental condition, the CTC formation does not take place when Al_2O_3 powders, calcinated at higher temperature (1100 °C) and forming an α-phase were used. For clarity, it should be emphasized that all results described in this work are obtained using exclusively Al_2O_3 powders with the γ-crystalline phase. Based on TGA measurements the content of organic phase in all inorganic/organic hybrids was found to be slightly smaller than 10 wt.-%.

The Kubelka-Munk transformations of diffuse reflection data for series of inorganic/organic hybrids: CAT/Al_2O_3, DHN/Al_2O_3, CA/Al_2O_3, DOPA/Al_2O_3, GA/Al_2O_3, SA/Al_2O_3, 5-ASA/Al_2O_3 and AA/Al_2O_3 are shown in Figure 4. The coordination of each of the above eight ligands, used to coat the surface of Al_2O_3 powder, induced the photon absorption in visible spectral range due to formation of CTCs as can be seen in Figure 4. Of course, depending on the ligands used, specific optical properties of obtained hybrids differ, and their effective band gap energies, determined from the absorption onset, are collected and listed in Table 1. Bearing in mind that the band gap value for pristine γ-Al_2O_3 is 8.7 eV [43], it is clear that CTC formation with any of the above ligands induces considerable red-shift in the onset of optical absorption. The largest shift was obtained for CAT (7.4 eV), while the smallest one was observed for SA (5.5 eV). The influence of functional side groups attached to the basic backbone structure of CAT is found to be relatively small. The largest difference in the effective band gap energies for inorganic/organic hybrids, prepared using catecholate-type of ligands, was found to be 200 meV (see Table 1 and compare data for CAT/Al_2O_3 and DHN/Al_2O_3) leaving limited ability to tune the optical properties by introducing different functional side groups to basic backbone structure of CAT. However, this is not the case with SA-type ligands: the difference between effective band gap energies of SA/Al_2O_3 and 5-ASA/Al_2O_3 is much larger (about 1.6 eV) in comparison to

differences observed among surface-modified Al_2O_3 powders with CAT-type of ligands. It should be stressed that, upon surface modification, accompanied by CTC formation, the optical properties of Al_2O_3, a typical insulator material, rank comparably with the optical properties of a semiconductor material.

The coordination, or the manner of attachment, of ligands to the Al_2O_3 surface was studied using FTIR spectroscopy. The FTIR spectra of free and adsorbed CAT and SA – i.e., ligands from which all other catecholate- and salicylate-type of ligands can be derived – are shown in Figure 5. In addition, the FTIR spectra of AA are also included in Figure 5. The FTIR spectra of other ligands, free and adsorbed, used in this study (DHN, CA, DOPA, GA and 5-ASA) are provided in Supporting Information 1. The FTIR spectrum of dried Al_2O_3 displays its characteristic broad bands in 4000−400 cm^{-1} region, and, consequently, it is possible to compare spectra of free and adsorbed ligands (CAT, SA and AA) in the desired spectral region. To this we turn now.

The fingerprint spectral region for CAT is from 1000 to 1700 cm^{-1}, and the main vibration bands and their assignments for free ligand (Figure 5A, curve a) are: stretching vibrations of the aromatic ring ν(C−C)/ν(C=C) at 1625, 1606, 1530, and 1475 cm^{-1}, stretching vibrations of the phenolic group ν(C−OH) at 1288, 1267, and 1250 cm^{-1}, bending vibrations of the phenolic group δ(C−OH) at 1374, 1201, 1169, and 1150 cm^{-1}, and bending δ(C−H) at 1100 and 1043 cm^{-1} [54–56]. Upon adsorption of CAT onto Al_2O_3 (curve b), the difference between FTIR spectra of free and adsorbed modifier is observed, signaling the formation of surface complex. Bending δ(C−OH) vibrations in the region below 1200 cm^{-1} and pronounced band at 1374 cm^{-1} nearly disappeared. Three bands of stretching vibrations ν(C−OH) merged into one prominent band at 1257 cm^{-1}. The binding of CAT to Al_2O_3 via two adjacent phenolic groups even affected the stretching of the aromatic ring (bands above 1400 cm^{-1}).

The FTIR spectra of SA, free and adsorbed on Al_2O_3 particles, are shown in Figure 5B. The main bands and their assignments in free SA (curve a) are well described in literature [57–61], and they are as follows: stretching vibrations of the aromatic ring ν(C−C)/ν(C=C) at 1621, 1583, 1492, 1472, and 1453 cm^{-1}, stretching vibrations of the phenolic group ν(C−OH) at 1265 cm^{-1}, bending vibrations of the phenolic group δ(C-OH) at 1386, 1329, 1217, and 1196 cm^{-1}, bending δ(C−H) at 1161, 1090, and 1031 cm^{-1}, stretching vibrations of CO in COOH ν(CO/COOH) at 1217 and 1196 cm^{-1} (both bands are coupled with δ(C–OH)), bending vibrations of CO in COOH δ(CO/COOH) at 1312 cm^{-1}, and pronounced stretching vibration of the carbonyl group ν(C=O) at 1693 cm^{-1}, existing only in the protonated form of acid. The adsorption of SA onto Al_2O_3 particles (curve b) leads to complete disappearance of the bands at 1693, 1492, 1329, 1265, and 1196 cm^{-1}. Since these bands correspond to vibrations of phenolic −OH and carboxylic −COOH group, it is obvious that both groups are coordinated (attached) to the surface Al atoms. The disappearance of stretching vibration of the carbonyl group ν(C=O) at 1693 cm^{-1} affirms the deprotonation of COOH group as the consequence of its binding to the surface Al atoms with the formation of delocalized carboxylate group [62]. The appearance of new band at 1580 cm^{-1} can be attributed to carboxylate asymmetric and symmetric stretching vibrations [57, 58].

Surface modification of Al_2O_3 with AA induces disappearance of the four stretching vibrations of the −OH groups that belong to the 2,3 enediole in the region from 3000 to 3500 cm^{-1} and the stretching vibration of the lactone group ν(C=O) at 1755 cm^{-1} (compare curves a and b in Figure 5C). On the other hand, the stretching vibration ν(C=C) at 1665 cm^{-1} was not affected, although its position was slightly shifted toward lower energies after the adsorption. Also, the complex semicircle stretch mode at 1380 cm^{-1}, where the top half of the ring stretches while the bottom half is contracting [63],[63] shows a slight increase in the energy of vibration. These results

indicate that AA is coordinated to the surface of Al_2O_3 over two neighboring –OH groups of the five-membered ring.

Based on the FTIR data, some general features can be readily recognized. First, upon coordination of ligands (CAT, SA, and AA) to the surface of Al_2O_3, the observed changes (disappearance, appearance, and shift of vibrational bands) are in agreement with published FTIR data concerning surface-modified TiO_2 nanoparticles with the same set of ligands [14, 15]. Second, the vibrational bands of catecholate-type of ligands (DHN, CA, DOPA, and GA) and 5-ASA changed in the same fashion as those of CAT and SA upon coordination to the Al_2O_3 surface, respectively (see Supporting Information 1). Third, from the FTIR data it is not possible to discriminate with certainty whether chelating or bridging mode of coordination between ligands and surface of the Al_2O_3 actually occurs. The existence of bridging coordination between these ligands and the surface in the case of TiO_2 nanoparticles was established by additional measurements that can only be performed with colloidal solutions [15–20], and, although bridging coordination is intuitively expected in our case, a more substantial evidence for this claim is needed.

3.2 DFT Calculations

On the theoretical side, the comprehensive DFT calculations were performed with periodic boundary conditions (PBC) in order to estimate the interfacial energy gaps of various L/Al_2O_3 complexes considered in this work. The calculations were performed by using Heyd-Scuseria-Ernzerhof screened-hybrid functional (HSE06) [47, 48], and the rationale for the choice of functional is discussed further below. It is known that the standard semi-local PBE functional underestimates the bandgaps for insulators and semiconductors [64, 65], although, this functional

describes with a high accuracy energy levels of interfacial charge-transfer between TiO_2 and catecholate-type of ligands [21]. On the other hand, the screened-hybrid density functional (HSE) predicts band-gaps for semiconductors and solids more precisely with no significant increase of the computational burden [66, 67]. However, it should be noted that all standard LDA and GGA functionals are not able to reproduce the band gap of bulk γ-Al_2O_3, and a proper electronic description has been achieved by using the modified semi-local Becke-Johnson exchange potential (mBJ) [68].

Our preliminary results for L/Al_2O_3 hybrids indicated reasonably good agreement between experimental and calculated band-gap values obtained using HSE06 functional and model systems based on bidentate coordination of ligand to (1 0 1) crystal surface [40]. Therefore, sophisticated model associated with (1 0 1) plane, previously benchmarked against CAT/Al_2O_3 system, at HSE06/6-31G(d,p) level, was used to calculate the position of electronic levels, as well as effective band gaps for the variety of L/Al_2O_3 complexes. The optimized structures of eight ligands anchored to the surface of γ-Al_2O_3 are shown in Figure 6, while the data concerning the relevant energy levels and band-gaps for these complexes are listed in Table 1. The data of the free ligands and unmodified γ-Al_2O_3 are also presented in Table 1. It should be noted that the valence band maximum (VBM) and the conduction band minimum (CBM) of unmodified γ-Al_2O_3 are located at -7.18 and -4.39 eV *vs.* AVS, respectively, yielding band-gap of 2.79 eV. Similar to other DFT-based methods (LDA[69] and GGA[70] functionals), HSE06 functional also failed to reproduce the band gap energy of bulk γ-Al_2O_3. It is evident that HOMO and HOMO-1 molecular levels of all ligands are positioned within the band gap region of γ-Al_2O_3 with exception of ascorbic acid (see Table 1), thus defining the two types of donor levels (α, β). Accordingly, the origin of interfacial charge-transfer transitions can be ascribed to excitation

from the donor level (α) to CBM of γ-Al_2O_3. In the case of ascorbic acid, the HOMO-1 orbital of free ligand lies below VBM, while associated donor level of AA/Al_2O_3 complex is slightly destabilized and positioned inside the band gap region of γ-Al_2O_3. In addition, the position of calculated LUMO orbitals for all ligands is significantly higher than CBM of γ-Al_2O_3 (Table 1). The description of energy structures of L/Al_2O_3 complexes, and origin of interfacial charge-transfer transitions, are in agreement with previous reports concerning surface-modified titanium dioxide with catecholate-type of ligands [21].

The excellent agreement between the calculated and experimental band-gap values was found for DOPA/Al_2O_3, CA/Al_2O_3 and DHN/Al_2O_3 inorganic/organic hybrids with deviation smaller than 5%. Practically, there is no difference between calculated and experimental band-gap values (compare, for example, 1.56 and 1.55 eV for DOPA/Al_2O_3). The small difference between calculated and experimental values was also found for AA/Al_2O_3 system – the calculated band-gap value is underestimated by only 0.06 eV compared with experimentally observed value. Larger discrepancies were found for two remaining members of studied catecholate's ligand family (less than 10 and 20% for CAT/Al_2O_3 and GA/Al_2O_3, respectively). However, significant differences between the calculated and experimental band-gap values were found for hybrids prepared using salicylate-type of ligands. The calculated band-gap values were underestimated by 31.6 and 18.7% compared to experimental ones for SA/Al_2O_3 and 5-ASA/Al_2O_3, respectively. It should be emphasized that all calculations were performed assuming bidentate bridging coordination of ligands. Most likely, the reason for significant discrepancies between calculated and experimental band gap data for SA/Al_2O_3 and 5-ASA/Al_2O_3 might be due to different coordination of salicylate-type of ligands onto the Al_2O_3 surface (chelating coordination and/or three points attachments including carboxylic functional group). Of course, the energies of

interfacial transitions are expected to be different for ligand molecules attached on different ways to the γ-Al_2O_3 surface.

In addition, the calculated band-gap data correctly follow ascending/descending order of experimentally determined band-gap values with exception of SA/Al_2O_3 hybrid, whose calculated value for interfacial energy transition is significantly underestimated compared to experimental one. The ability of electron-donating and/or electron-withdrawing side functional groups to decrease/increase the band-gap energy of inorganic/organic hybrids is well-established in literature [21, 27]. In this particular case, calculated band-gap values for CAT/Al_2O_3 and CA/Al_2O_3 are very close to each other (1.38 and 1.34 eV, respectively), and only this pair of hybrids has inverse order of band-gap values compared to experimental ones (1.26 and 1.41 eV for CAT/Al_2O_3 and CA/Al_2O_3, respectively). At present, we do not have convincing argument to explain such findings.

The spatial distribution of crystal orbitals of SA/Al_2O_3, AA/Al_2O_3, CA/Al_2O_3, and unmodified γ-Al_2O_3, as well as frontier orbitals of the free SA molecule are shown in Figure 7, whereas the results concerning the orbital electron densities of other CTCs are presented in Supporting Information 2. It is evident from the Figure 7 that the VBM and CBM orbitals of unmodified γ-Al_2O_3 coincide with those of coordinated Al_2O_3 complexes. The ligand orbitals related with HOMO-1 and HOMO, which mostly consist of aromatic π-orbitals, are positioned between VBM and CBM. In the case of CAT/Al_2O_3, CA/Al_2O_3 and DOPA/Al_2O_3, the β-levels are not composed of only HOMO orbitals of ligands, but it is somewhat delocalized over the lattice atoms (see Figure 7 and Supporting Information 2), which may be the likely cause for their additional stabilization.

It is well-known that the efficient photocatalyst, in addition to its capability to harvest large portion of solar spectrum, determined by the band gap energy, must have a proper position of the valence and conduction bands, because the potentials of valence and conduction band are the measure of its oxidation and reduction ability, respectively. For this purpose, the DFT results obtained at the HSE06/6-31G(d,p) level of theory for donor level and CBM potentials are presented at electrochemical scale with respect to normal hydrogen electrode, as illustrated in Figure 8. Our preliminary results indicate that surface-modified Al_2O_3 particles with 5-ASA have the ability to induce photocatalytic degradation of organic dye methylene blue [40]. However, our attempt to produce hydrogen using synthesized inorganic/organic hybrids failed. These results support calculated energy alignment of studied CTCs. The obtained experimental results, supported with detailed DFT calculations, represent the solid basis to further extend these studies to a variety of photo-driven processes.

4 Conclusions

In conclusion, we have synthesized a number of Al_2O_3 organic/inorganic hybrids and thoroughly analyzed their optical properties by experimental and theoretical methods. Our results indicate that the CTC formation, accompanied with the red-shifted onset of optical absorption, is not exclusive to solar light absorbing oxides (TiO_2, ZnO, $Na_2Ti_3O_7$, Mg_2TiO_4 and $BaTiO_3$). We have demonstrated that coordination of small colorless organic molecules with specific functionality (catecholate- and salicylate-type of ligands, as well as ascorbic acid) to solar light non-absorbing Al_2O_3 insulator with proper structure and morphology leads to the formation of inorganic/organic hybrids whose optical properties can be tuned throughout Vis and even high-energy part of NIR

spectral region. The additional advantage of these novel low-cost hybrid materials is that the procedure needed for their synthesis is quite simple and reproducible.

Supporting Information

Supporting Information 1: Vibrational bands of catecholate-type of ligands (DHN, CA, DOPA, and GA) and 5-ASA changed upon coordination to the Al_2O_3 surface, respectively (see Figure S1. FTIR spectra of free (a) and adsorbed (b) ligands on Al_2O_3 powders: (A) DHN, and (B) CA, (C) DOPA, (D) GA , and (E) 5-ASA).

Supporting Information 2: The spatial distribution of crystal orbitals of CAT/Al_2O_3, GA/Al_2O_3, DOPA/Al_2O_3, DHN/Al_2O_3, and 5-ASA /Al_2O_3. (see Figure S2. The frontier crystal orbitals drawn over a single repeated unit for L/Al_2O_3 complexes (L = CAT, GA, DOPA, DHN, 5-ASA). HOCO and LUCO represent highest occupied and lowest unoccupied crystal orbitals.

Acknowledgement

Financial support for this study is supported by the Ministry of Education, Science and Technological Development of the Republic of Serbia (project 45020). Work at the Texas A&M University at Qatar was made possible by NPRP grants 7-665-1-125 and 7-245-1-035 from the Qatar National Research Fund.

References

[1] A. Fujishima, K. Honda, Electrochemical photolysis of water at a semiconductor electrode, Nature, 238, 37–38 (1972).

[2] E. Pelizzetti, C. Minero, Metal oxides as photocatalysts for environmental detoxification, Comments Inorg. Chem., 15, 297–337 (1994).

[3] M.R. Hoffman, S.T. Martin, W.Y. Choi, D.W. Bahnemann, Environmental applications of semiconductor photocatalysis, Chem. Rev., 95, 69–96 (1995).

[4] B. Ohtani, Photocatalysis A to Z: What we know and what we do not know in a scientific sense, J. Photoch. Photobio. C, 11, 157–178 (2010).

[5] A.B. Djurišić, Y.H. Leung, A.M.C. Ng, Strategies for improving the efficiency of semiconductor metal oxide photocatalysis, Mater. Horiz., 1, 400–410 (2014).

[6] H. Wang, L. Zhang, Z. Chen, J. Hu, S. Li, Z. Wang, J. Liu, X. Wang, Semiconductor heterojunction photocatalysts: design, construction, and photocatalytic performances, Chem. Soc. Rev., 43, 5234–5244 (2014).

[7] T. Rajh, N.M. Dimitrijevic, M. Bissonnette, T. Koritarov, V. Konda, Titanium dioxide in the service of the biomedical revolution, Chem. Rev., 114, 10177−10216 (2014).

[8] B. O'Regan, M. Grätzel, A low-cost, high-efficiency solar cell based on dye-sensitized colloidal TiO_2 films. Nature, 353, 737–740 (1991).

[9] M. Zhang, C.C. Chen, W.H. Ma, J.C. Zhao, Visible-light-induced aerobic oxidation of alcohols in a coupled photocatalytic system of dye-sensitized TiO_2 and TEMPO, Angew. Chem. Int. Ed., 47, 9730–9733(2008).

[10] R. Asahi, T. Morikawa, K. Aoki, Y. Taga, Visible-light photocatalysis in nitrogen-doped titanium oxides, Science, 293, 269–271 (2001).

[11] S. Sakthivel, H. Kisch, Angew. Daylight Photocatalysis by carbon-modified titanium dioxide, Chem. Int. Ed., 42, 4908–4911 (2003).

[12] Y. Tian, T. Tatsuma, Mechanisms and applications of plasmon-induced charge separation at TiO_2 films loaded with gold nanoparticles, J. Am. Chem. Soc., 127, 7632–7637 (2005).

[13] S. Naya, K. Kimura, H. Tada, One-step selective aerobic oxidation of amines to imines by gold nanoparticle-loaded rutile titanium(iv) oxide plasmon photocatalyst, ACS Catal., 3, 10–13 (2013).

[14] T. Rajh, J.M. Nedeljković, L.X. Chen, O. Poluetkov, M.C Thurnauer, Improving optical and charge separation properties of nanocrystalline TiO_2 by surface modification with vitamin C, J. Phys. Chem. B, 103, 3515–3519 (1999).

[15] I.A. Janković, Z.V Šaponjić, M.I. Čomor, J.M. Nedeljković, Surface modification of colloidal TiO_2 nanoparticles with bidentate benzene derivatives, J. Phys. Chem. C, 113, 12645–12652 (2009).

[16] I.A. Janković, Z.V. Šaponjić, E.S. Džunuzović, J.M. Nedeljković, New hybrid properties of TiO_2 nanoparticles surface modified with catecholate type ligands, Nanoscale Res. Lett., 5, 81−88 (2010).

[17] T.D. Savić, I.A. Janković, Z.V. Šaponjić, M.I. Čomor, D.Ž. Veljković, S.D. Zarić, J.M. Nedeljković, Surface modification of anatase nanoparticles with fused catecholate type ligands: a combinated DFT and experimental study of optical properties, Nanoscale, 4, 1612–1619 (2012).

[18] T.D. Savić, Z.V. Šaponjić, M.I. Čomor, J.M. Nedeljković, M.D. Dramićanin, M.G. Nikolić, D.Ž. Veljković, S.D. Zarić, I.A. Janković, Surface modification of anatase nanoparticles fused ring salicylate-type ligands (3-hydroxy-2-naphthoic acids): a combined DFT and experimental study of optical properties, Nanoscale, 5, 7601–7612 (2013).

[19] T.D. Savić, M.I. Čomor, J.M. Nedeljković, D.Ž. Veljković, S.D. Zarić, V.M. Rakić, I.A. Janković, The effect of substituents on the surface modification of anatase nanoparticles with catecholate-type ligands: a combined DFT and experimental study, Phys. Chem. Chem. Phys., 16, 20796–20805 (2014).

[20] T.D. Savić, M.I. Čomor, N.D. Abazović, Z.V. Šaponjić, M.T. Marinović-Cincović, D.Ž. Veljković, S.D. Zarić, I.A. Janković, Anatase nanoparticles surface modified with fused ring salicylate-type ligands (1-hydroxy-2-naphthoic acids): a combined DFT and experimental study, J. Alloy Compd., 630, 226–235 (2015).

[21] S. Higashimoto, T. Nishi, M. Yasukawa, M. Azuma, Y. Sakata, H. Kobayashi, Photocatalysis of titanium dioxide modified by catechol-type interfacial surface complexes (ISC) with substitued groups, J. Catal., 329, 286–290 (2015).

[22] T. Zhang, P. Wojtal, O. Rubel, I. Zhitomirsky, Density functional theory and experimental studies of caffeic acid adsorption on zinc oxide and titanium dioxide nanoparticles, RSC Adv., 5, 106877 (2015).

[23] R.J. Wilkerson, T. Elder, O. Sowinksi, J.I. Fostvedt, J.D. Hoefelmeyer, Phase transfer of oleic acid stabilized rod-shaped anatase TiO_2 nanocrystals, Surf. Sci., 648, 333–338 (2016).

[24] B. Moongraksathum, P-T. Hsu, Y-W. Chen, Photocatalytic activity of ascorbic acid-modified TiO_2 sol prepared by the peroxo sol–gel method, J. Sol-Gel Sci. Technol., 78, 647–659 (2016).

[25] D. Finkelstein-Shapiro, S.K. Davidowski, P. Lee, C. Guo, G.P. Holland, T. Rajh, K.A. Gray, J.L. Yarger, M. Calatayud, Direct evidence of chelated geometry of Catechol on TiO_2 by a combined solid state NMR and DFT study, J. Phys. Chem. C, 120, 23625−23630 (2016).

[26] J. Fujisawa, S. Matsumura, M. Hanaya, A single Ti-O-C linkage induces interfacial charge-transfer transitions between TiO_2 and a π-conjugated molecule, Chem. Phys. Lett., 657, 172−176 (2016).

[27] D.N. Sredojević, T. Kovač, E. Džunuzović, V. Đorđević, B.N. Grgur, J.M. Nedeljković, Surface-modified TiO_2 powders with phenol derivatives: A comparative DFT and experimental study, Chem. Phys. Lett., 686, 167–172 (2017).

[28] I.M. Dugandžić, D.J. Jovanović, L.T. Mančić, N. Zheng, S.P. Ahrenkiel, O.B. Milošević, Z.V. Šaponjić, J.M. Nedeljković, Surface modification of submicronic TiO_2 particles prepared by ultrasonic spray pyrolysis for visible light absorption, J. Nanopart. Res., 14, 1157−1167 (2012).

[29] I.M. Dugandžić, D.J. Jovanović, L.T. Mančić, O.B. Milošević, S.P. Ahrenkiel, Z.V. Šaponjić, J.M. Nedeljković, Ultrasonic spray pyrolysis of surface modified TiO_2 nanoparticles with dopamine, Mater. Chem. Phys., 143, 233−239 (2013).

[30] B. Milićević, V. Đorđević, D. Lončarević, S.P. Ahrenkiel, M.D. Dramićanin, J.M. Nedeljković, Visible light absorption of surface modified TiO_2 powders with bidentate benzene derivatives, Micropor. Mesopor. Mat., 217, 184–189 (2015).

[31] I. Vukoje, T. Kovač, J. Džunuzović, E. Džunuzović, D. Lončarević, S.P. Ahrenkiel, J.M. Nedeljković, Photocatalytic ability of visible-light-responsive TiO_2 nanoparticles, J. Phys. Chem. C, 120, 18560−18569 (2016).

[32] B. Yao, C. Peng, P. Lu, Y. He, W. Zhang, Q. Zhang, Fabrication of Tiron-TiO_2 charge-transfer complex with excellent visible-light photocatalytic performance, Mater. Chem. Phys., 184, 298−305 (2016).

[33] S. Günes, N. Marjanović, J.M. Nedeljković, N.S. Sariciftci, Photovoltaic characterization of hybrid solar cells using surface modified TiO_2 nanoparticles and poly(3-hexyl)thiophene, Nanotechnology, 19, 424009 (2008).

[34] S. Manzhos, Comparative density functional theory and density functional tight binding study of 2-anthroic acid on TiO_2, Chem. Phys. Lett., 643, 16–20 (2016).

[35] S. Manzhos, K. Kotsis, Computational study of interfacial charge transfer complexes of 2-anthroic acid adsorbed on a titania nanocluster for direct injection solar cells, Chem. Phys. Lett., 660, 69–75 (2016).

[36] L. Tian, J. Xu, A. Alnafisah, R. Wang, X. Tan, N.A. Oyler, L. Liu, X. Chen, A novel green TiO_2 photocatalyst with surface charge-transfer complex of Ti and hydrazine groups, Chem. Eur. J., 23, 5345–5351 (2017).

[37] D. Jaušovec, M. Božič, J. Kovač, J. Štrancar, V. Kokol, Synergies of phenolicacids' surface-modified titanate nanotubes (TiNT) for enhanced photo-catalytic activities, J. Colloid Interf. Sci., 438, 277–290 (2015).

[38] M.M. Medić, M. Vasić, A.R. Zarubica, L.V. Trandafilović, G. Dražić, M.D. Dramićanin, J.M. Nedeljković, Enhanced photoredox chemistry in surface-modified Mg_2TiO_4 nano-powders with bidentate benzene derivatives, RSC Adv., 6, 94780–94786 (2016).

[39] J. Fujisawa, T. Eda, M. Hanaya, Interfacial charge-transfer transitions in $BaTiO_3$, J. Phys. Chem. C, 120, 21162–21168 (2016).

[40] V. Đorđević, J. Dostanić, D. Lončarević, S.P. Ahrenkiel, D.N. Sredojević, N. Švrakić, M. Belić, J.M. Nedeljković, Hybrid visible-light responsive Al_2O_3 particles, Chem. Phys. Lett., 685, 416–421 (2017).

[41] J. Čejka, Organized mesoporous alumina: synthesis, structure and potential in catalysis, App. Catal. A Gen., 254, 327−338 (2003).

[42] C. Márquez-Alvarez, N. Žilková, J. Pérez-Pariente, J. Čejka, Synthesis, characterization and catalytic applications of organized mesoporous aluminas, Cat. Rev. Sci. Eng., 50, 222−286 (2008).

[43] B. Ealet, M.H. Elyakhloufi, E. Gillet, M. Ricci, Electronic and crystallographic structure of γ-alumina thin films, Thin Solid Films, 250, 92–100 (1994).

[44] W. Wu, Z. Wan, W. Chen, M. Zhu, D. Zhang, Synthesis of mesoporous alumina with tunable structural properties, Micropor. Mesopor. Mat., 217, 12–20 (2015).

[45] S. Brunauer, P.H. Emmett, E. Teller, Adsorption of gases in multimolecular layers, J. Am. Chem. Soc., 60, 309–319 (1938).

[46] M.J. Frisch, G.W. Trucks, H.B. Schlegel, G.E. Scuseria, M.A. Robb, J.R. Cheeseman, G. Scalmani, V. Barone, B. Mennucci, G.A. Petersson, H. Nakatsuji, M. Caricato, X. Li, H.P. Hratchian, A.F. Izmaylov, J. Bloino, G. Zheng, J.L. Sonnenberg, M. Hada, M. Ehara, K. Toyota, R. Fukuda, J. Hasegawa, M. Ishida, T. Nakajima, Y. Honda, O. Kitao, H. Nakai, T. Vreven, J.A. Montgomery, J.E. Peralta, F. Ogliaro, M. Bearpark, J.J. Heyd, E. Brothers, K.N. Kudin, V.N. Staroverov, R. Kobayashi, J. Normand, K. Raghavachari, A. Rendell, J.C. Burant, S.S. Iyengar, J. Tomasi, M. C ossi, N. Rega, J.M. Millam, M. Klene, J.E. Knox, J.B. Cross, V. Bakken, C. Adamo, J. Jaramillo, R. Gomperts, R.E. Stratmann, O. Yazyev, A.J. Austin, R. Cammi, C. Pomelli, J.W. Ochterski, R.L. Martin, K. Morokuma, V.G. Zakrzewski, G.A. Voth, P. Salvador, J.J. Dannenberg, S. Dapprich, A.D. Daniels, O. Farkas, J.B. Foresman, J.V. Ortiz, J. Cioslowski, D.J. Fox, Gaussian 09, Revision B.01; Gaussian, Inc.: Wallingford, CT, 2010.

[47] J. Heyd, G. E. Scuseria, M. Ernzerhof, Hybrid functionals based on a screened Coulomb potential, J. Chem. Phys., 118, 8207–8215 (2003).

[48] J. Heyd, G. E. Scuseria, Assessment and validation of a screened Coulomb hybrid density functional, J. Chem. Phys., 120, 7274–7280 (2004).

[49] R. Ditchfield, W.J. Hehre, J.A. Pople, Self-consistent molecular orbital methods. IX. Extended Gaussian-type basis for molecular-orbital studies of organic molecules, J. Chem. Phys., 54, 724–728 (1971).

[50] W.J. Hehre, R. Ditchfield, J.A. Pople, Self-Consistent Molecular Orbital Methods. XII. Further extensions of Gaussian-type basis sets for use in molecular-orbital studies of organic-molecules, J. Chem. Phys., 56, 2257–2261 (1972).

[51] H.J. Monkhorst, J.D. Pack, Special points for Brillouin-zone integrations, Phys. Rev. B, 13, 5188–5192 (1976).

[52] S. Cava, S.M. Tebcherani, I.A. Souza, S.A. Pianaro, C.A. Paskocimas, E. Longo, J.A. Varela, Structural characterization of phase transition of Al_2O_3 nanopowders obtained by polymeric precursor method, Mater. Chem. Phys., 103, 394–399 (2007).

[53] E.P. Barret, L.G. Joyner, P.P. Halenda, The determination of pore volume and area distributions in porous substances. I. Computations from nitrogen isotherms, J. Am. Chem. Soc., 73, 373–380 (1951).

[54] P.A. Connor, K.D. Dobson, A.J. McQuillan, New sol-gel attenuated total reflection infrared spectroscopic method for analysis of adsorption at metal oxide surfaces in aqueous solutions. Chelation of TiO_2, ZrO_2, and A_2O_3 Surfaces by Catechol, 8-Quinolinol, and Acetylacetone, Langmuir, 11, 4193−4195 (1995).

[55] P.Z. Araujo, C.B. Mendive, L.A. Garcia Rodenas, P.J. Morando, A.E. Regazzoni, M.A. Blesa, D. Bahnemann, FT-IR–ATR as a tool to probe photocatalytic interfaces, Coll. Surf. A, 265, 73−80 (2005).

[56] P.Z. Araujo, P.J. Morando, M.A. Blesa, Interaction of Catechol and Gallic acid with Titanium dioxide in aqueous suspensions. 1. Equilibrium Studies, Langmuir, 21, 3470−3474 (2005).

[57] E.C. Yost, M.I. Tejedor-Tejedor, M.A. Anderson, In situ CIR-FTIR characterization of salicylate complexes at the goethite/aqueous solution interface, EnViron. Sci. Technol., 24, 822−828 (1990).

[58] S. Tunesi, M.A, Anderson, Surface effects in photochemistry: an in situ cylindrical internal reflection-Fourier transform infrared investigation of the effect of ring substituents on chemisorption onto titania ceramic membranes, Langmuir, 8, 487−495 (1992).

[59] A.D. Weisz, L. Garcia Rodenas, P.J. Morando, A.E. Regazzoni, M.A. Blesa, FTIR study of the adsorption of single pollutants and mixtures of pollutants onto titanium dioxide in water: oxalic and salicylic acids, Catal. Today, 76, 103−112 (2002).

[60] L. Jiang, L. Gao, Y. Liu, Adsorption of salicylic acid, 5-sulfosalicylic acid and Tiron at the alumina–water interface, Colloid Surface A, 211, 165−172 (2002).

[61] X. Guan, G. Chen, C. Shang, ATR-FTIR and XPS study on the structure of complexes formed upon the adsorption of simple organic acids on aluminum hydroxide, J. EnViron. Sci., 19, 438−443 (2007).

[62] M.V. Biber, W. Stumm, An in-situ ATR-FTIR study: The surface coordination of salicylic acid on aluminum and iron (III) oxides, EnViron. Sci. Technol., 28, 763−768 (1994).

[63] D. Lin-Viem, N.B. Colthap, W.G. Fateley, J.G. Grasselli, Infrared and Raman Characteristic Frequencies of Organic Molecules, Academic Press: San Diego, 1991.

[64] J.M. Crowley, J. Tahir-Kheli, W.A. Goddard, Resolution of the band gap prediction problem for materials design, J. Phys. Chem. Lett., 7, 1198–1203 (2016).

[65] J. Lee, A. Seko, K. Shitara, K. Nakayama, I. Tanaka, Prediction model of band gap for inorganic compounds by combination of density functional theory calculations and machine learning techniques, Phys. Rev. B, 93, 115104 (2016).

[66] J.E. Moussa, P.A. Schultz, J.R. Chelikowsky, Analysis of the Heyd-Scuseria-Ernzerhof density functional parameter space, J. Chem. Phys., 136, 204117 (2012).

[67] E.N. Brothers, A.F. Izmaylov, J.O. Normand, V. Barone, G.E. Scuseria, Accurate solid-state band gaps via screened hybrid electronic structure calculations, J. Chem. Phys., 129, 011102 (2008).

[68] M. Yazdanmehr, S.J. Asadabadi, A. Nourmohammadi, M. Ghasemzadeh, M. Rezvanian, Electronic structure and bandgap of γ-Al_2O_3 compound using mBJ exchange potential, Nanoscale Res. Lett., 7, 488 (2012).

[69] E. Menéndez-Proupin, G. Gutiérrez, Electronic properties of bulk γ-Al_2O_3, Phys. Rev. B, 72, 035116 (2005).

[70] H.P. Pinto, R.M. Nieminen, S.D. Elliott, *Ab initio* study of γ-Al_2O_3 surfaces, Phys. Rev. B, 70, 125402 (2004).

Table 1. The energies of frontier orbitals (in eV) of eight different ligands, γ-Al_2O_3 and L/Al_2O_3 complexes calculated by DFT using PBC model, as well as energy gaps of free ligands and corresponding inorganic/organic hybrids. For comparison reasons experimentally determined optical gaps are included. (VBM – valence band maximum; CBM – conduction band minimum).

STRUCTURE	VBM	Donor level (α)	HOMO-1	Donor level (β)	HOMO	CBM	LUMO	E_g^{calc}	E_g^{exp}
CAT/Al_2O_3	-7.64	-6.39	-	-6.14	-	-5.01	-	1.38	1.26
CAT	-	-	-6.33	-	-5.48	-	0.02	5.50*	
SA/Al_2O_3	-7.62	-7.21	-	-6.72	-	-5.00	-	2.21	3.23
SA	-	-	-7.20	-	-6.39	-	-1.57	4.82*	
AA/Al_2O_3	-7.45	-7.25	-	-5.96	-	-4.83	-	2.42	2.48
AA	-	-	-7.63	-	-5.97	-	-0.84	5.13*	
CA/Al_2O_3	-7.80	-6.62	-	-6.50	-	-5.28	-	1.34	1.41
CA	-	-	-6.64	-	-5.89	-	-2.04	3.85*	
GA/Al_2O_3	-7.24	-6.56	-	-6.21	-	-4.82	-	1.74	2.10
GA	-	-	-6.26	-	-5.82	-	-1.40	4.42*	
DOPA/Al_2O_3	-7.48	-6.61	-	-6.18	-	-5.05	-	1.56	1.55
DOPA	-	-	-6.22	-	-5.41	-	-0.26	5.15*	
DHN/Al_2O_3	-7.58	-6.57	-	-6.49	-	-5.14	-	1.43	1.45
DHN	-	-	-5.76	-	-5.62	-	-1.23	4.39*	
5-ASA/Al_2O_3	-7.51	-7.04	-	-6.56	-	-5.07	-	1.97	1.66
5-ASA	-	-	-6.80	-	-6.21	-	1.53	4.68*	
γ-Al_2O_3	-7.18	-	-	-	-	-4.39	-	2.79	8.7**

*HOMO–LUMO gaps.

**The band gap value for bulk Al_2O_3 was taken from reference [43].

Figure Captions

Figure 1. The wide-angle XRD patterns of Al_2O_3 particles prepared by a sol-gel process via hydrolysis of aluminum isopropoxide, followed with calcination at: (A) 700 °C, and (B) 1100 °C with the corresponding JCPDS cards.

Figure 2. TEM data from γ-Al_2O_3 powders: typical bright- (A) and dark-field (B) TEM images of γ-Al_2O_3 powders, high-magnification TEM image (C), and corresponding SAED pattern (D).

Figure 3. The nitrogen adsorption-desorption isotherms (a), and pore size distribution (b) of γ-Al_2O_3 powders.

Figure 4. Kubelka–Munk transformations of UV-Vis-NIR diffuse reflection data of inorganic/organic hybrids: CAT/Al_2O_3, DHN/Al_2O_3, CA/Al_2O_3, DOPA/Al_2O_3, GA/Al_2O_3, SA/Al_2O_3, 5-ASA/Al_2O_3 and AA/Al_2O_3.

Figure 5. FTIR spectra of free (a) and adsorbed (b) ligands on Al_2O_3 powders: (A) CAT, and (B) SA, and (C) AA.

Figure 6. The optimized geometries of eight different L/Al_2O_3 complexes used in periodic calculations. The alignment of molecular slabs for (101)-surface is also presented.

Figure 7. The frontier crystal orbitals drawn over a single repeated unit for L/Al_2O_3 complexes (L = SA, AA, CA). The orbitals of free SA molecule, as well as VBM and CBM of unmodified γ-Al_2O_3 are also presented. HOCO and LUCO represent highest occupied and lowest unoccupied crystal orbitals.

Figure 8. The donor level and CBM energy alignment for the considered CTCs with respect to the band gap redox potential for H_2 and O_2 evolution.

Figure S1. FTIR spectra of free (a) and adsorbed (b) ligands on Al_2O_3 powders: (A) DHN, and (B) CA, (C) DOPA, (D) GA , and (E) 5-ASA.

Figure S2. The frontier crystal orbitals drawn over a single repeated unit for L/Al_2O_3 complexes (L = CAT, GA, DOPA, DHN, 5-ASA). HOCO and LUCO represent highest occupied and lowest unoccupied crystal orbitals.

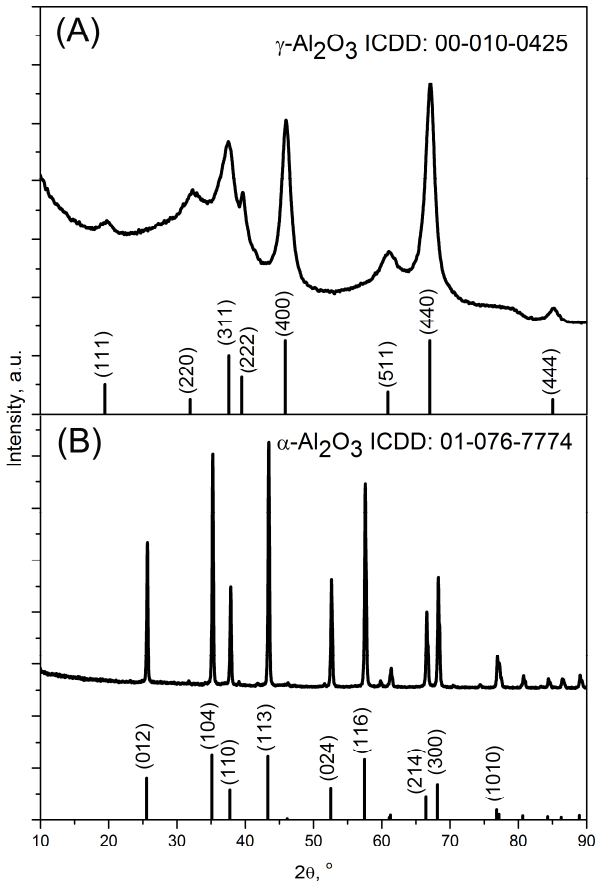

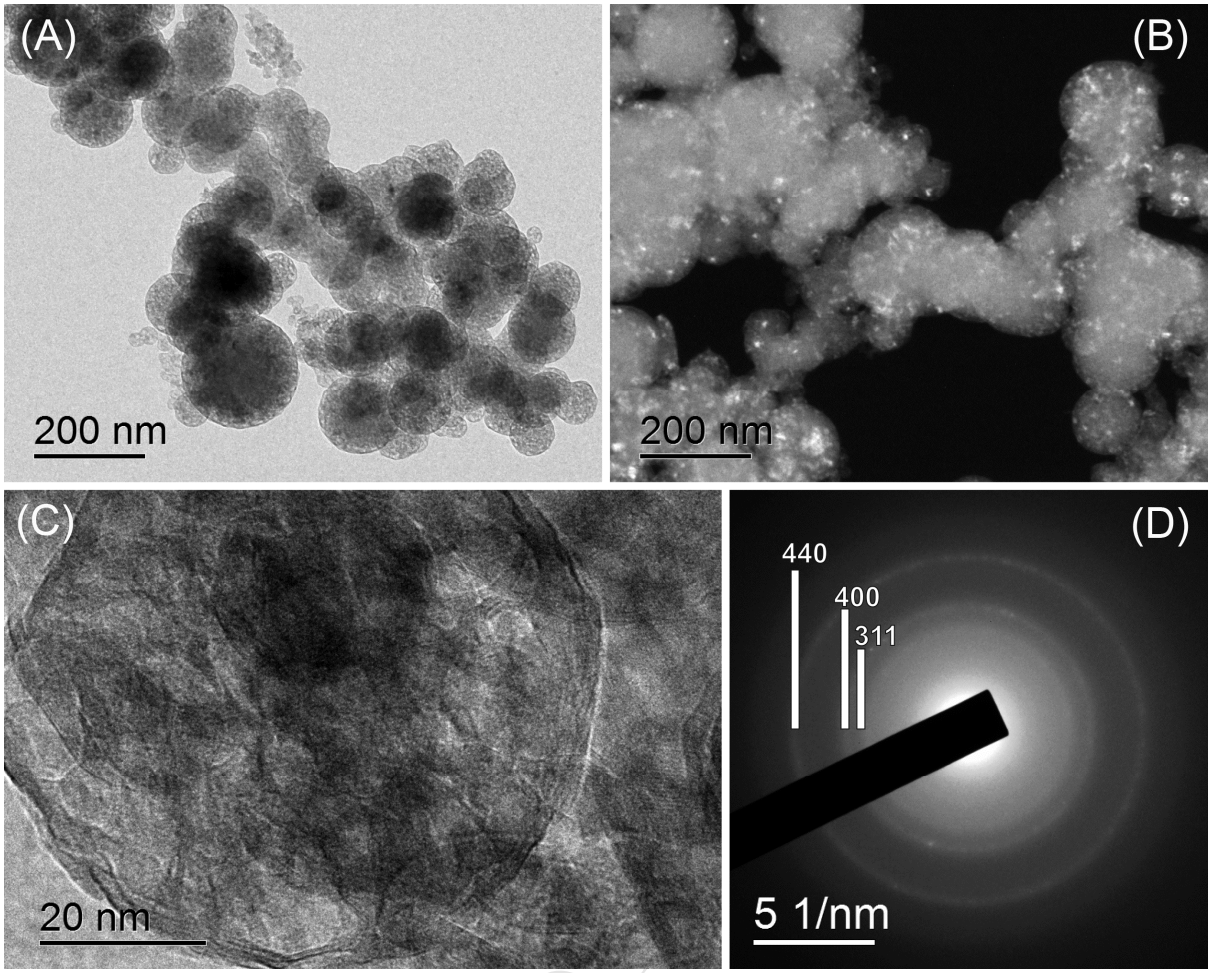

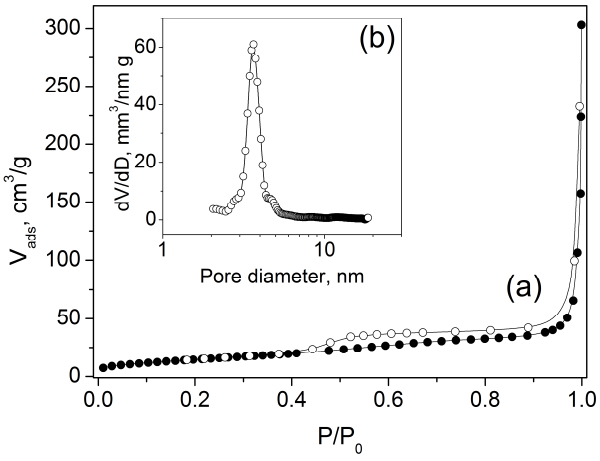

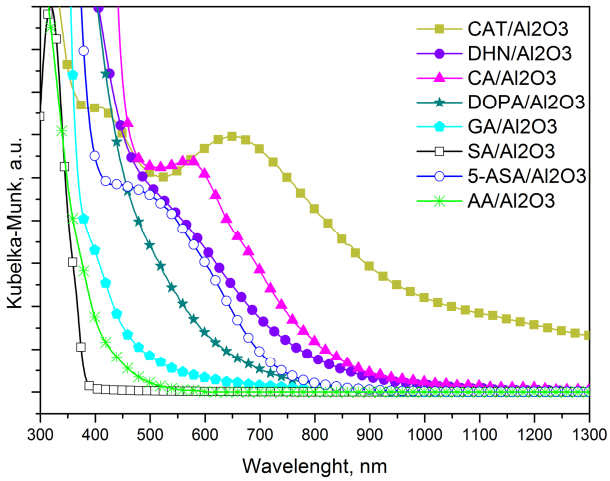

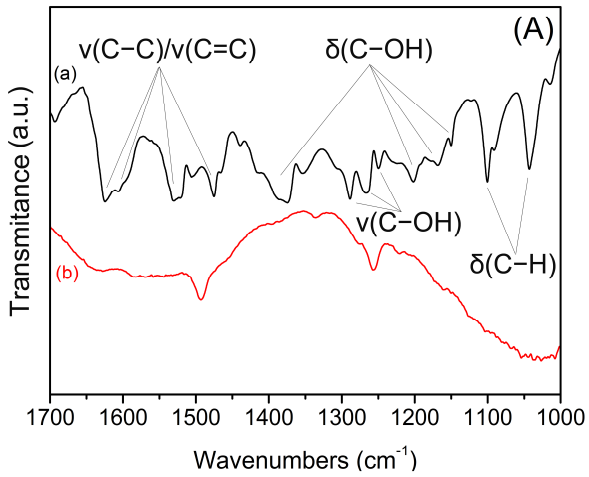

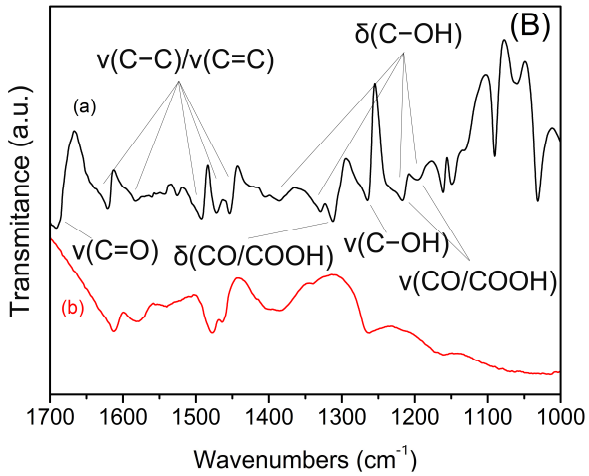

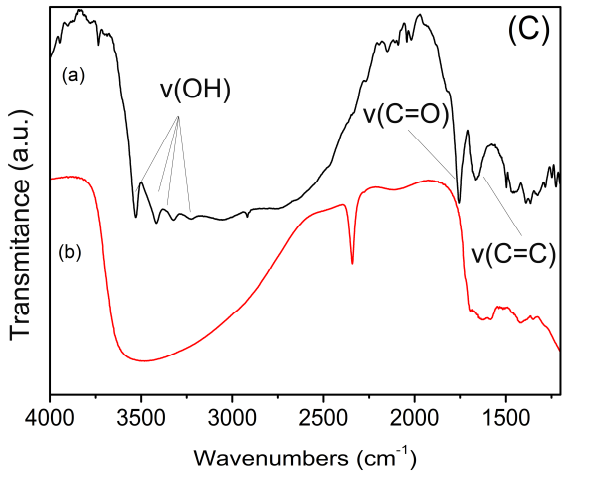

CAT/Al_2O_3

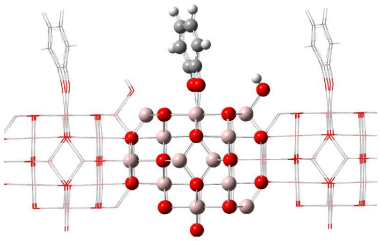

SA/Al_2O_3

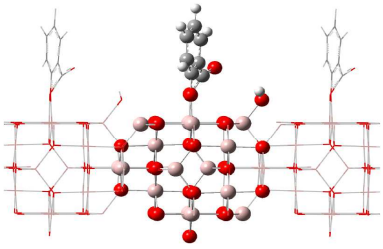

AA/Al_2O_3

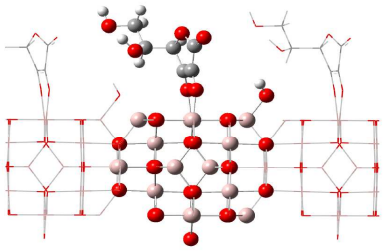

CA/Al_2O_3

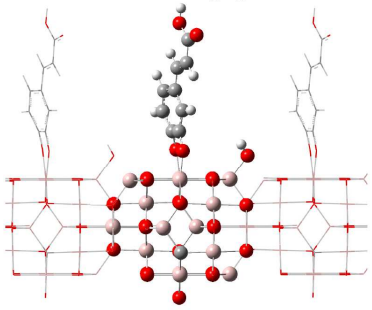

GA/Al_2O_3

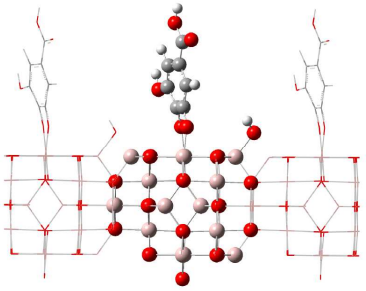

DOPA/Al_2O_3

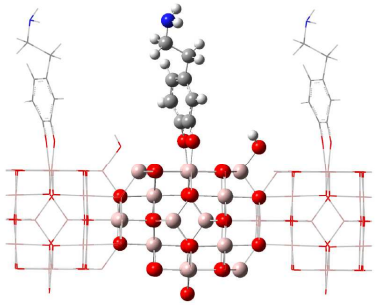

DHN/Al_2O_3

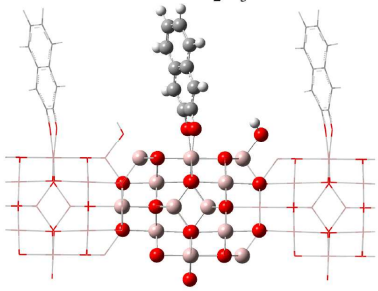

5-ASA/Al_2O_3

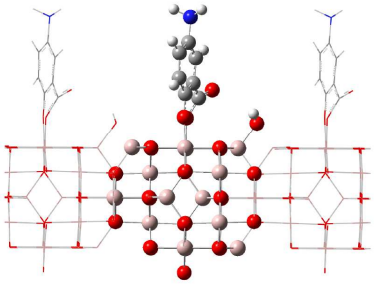

γ-Al_2O_3

101 - surface

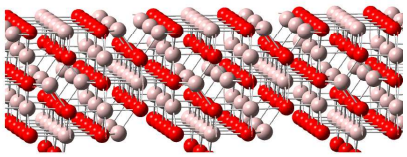

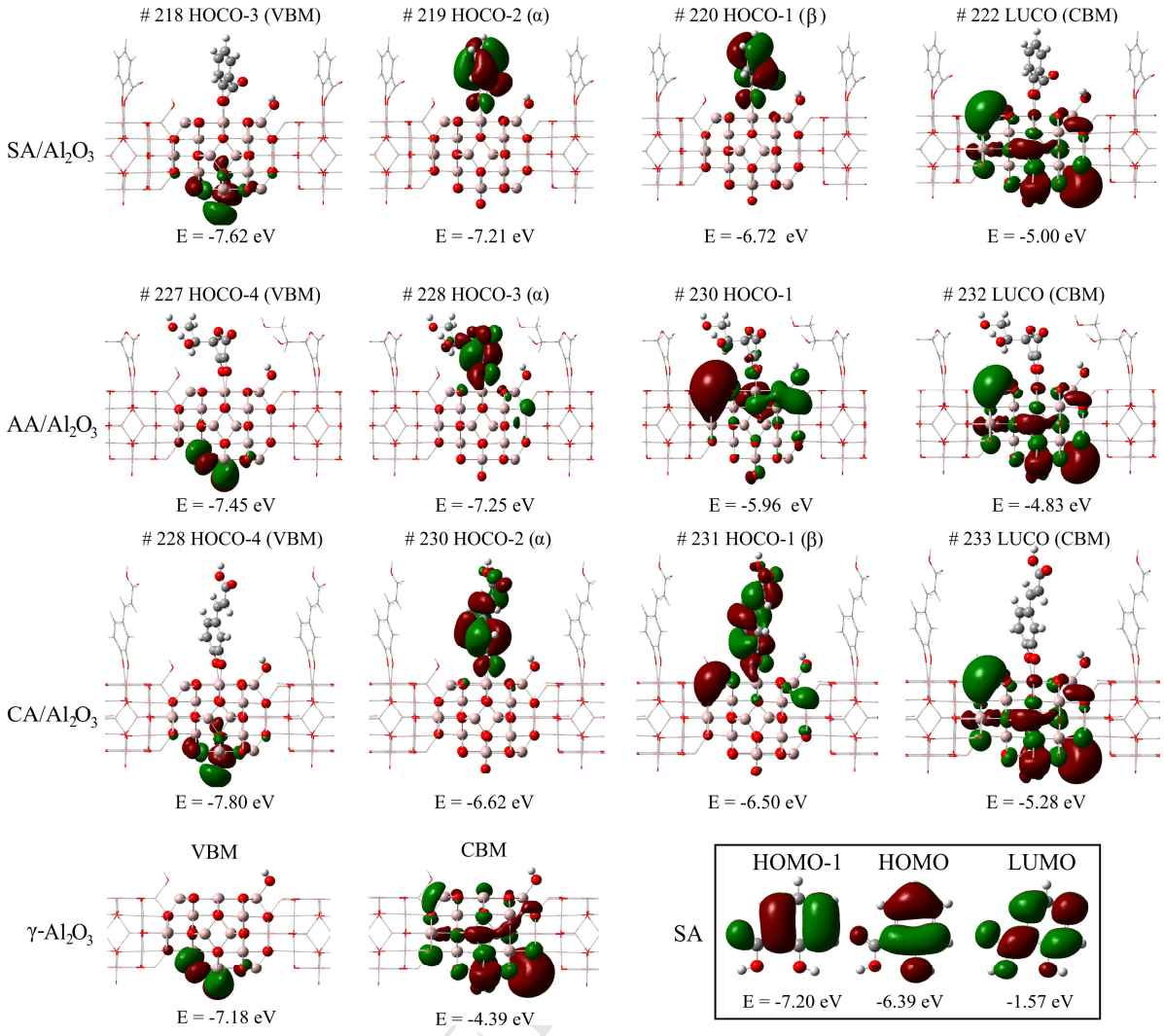

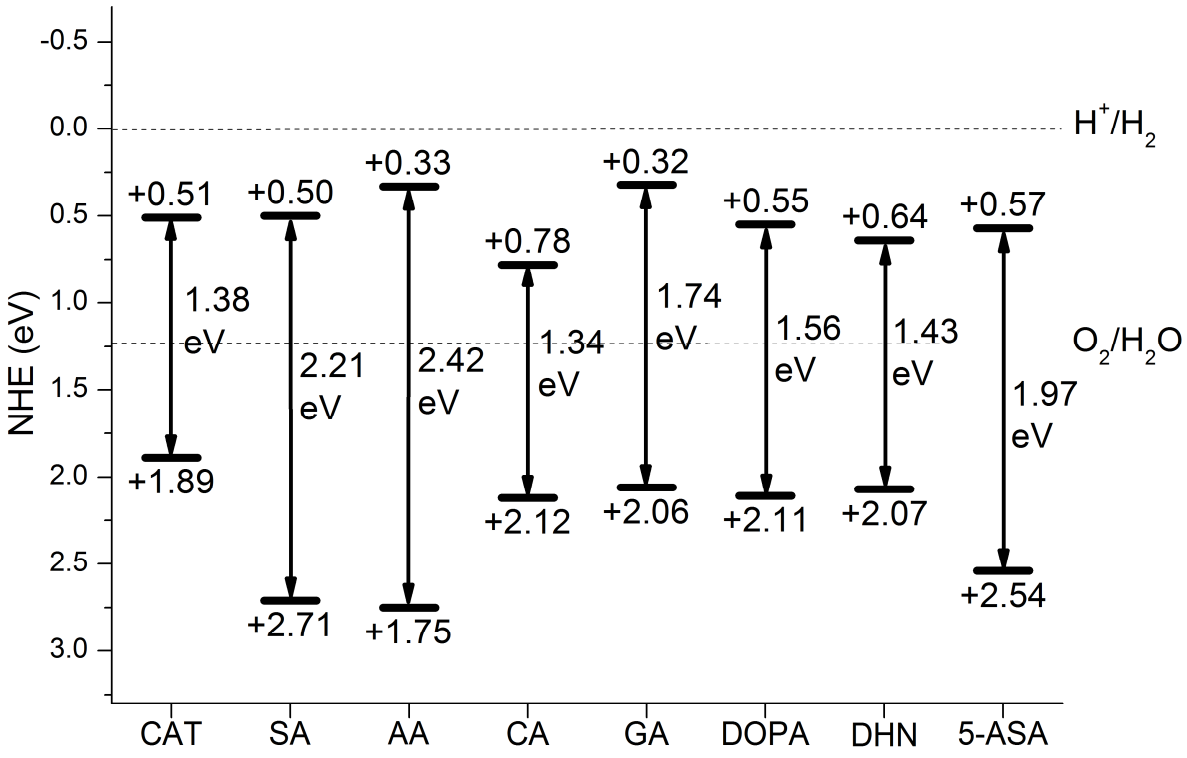

- Surface modification of mesoporous Al_2O_3 powder with benzene derivatives
- Charge transfer complex formation between Al_2O_3 and small colorless organic molecules
- Visible-light activity of surface-modified Al_2O_3 powders
- Large-scale quantum chemical calculations based on density functional theory